13.2

HIGH-TEMPORAL RESOLUTION GROUND-BASED OBSERVATIONS OF AN EASTERN KANSAS BORE DURING THE PECAN FIELD CAMPAIGN

David M. Loveless*, Nadia Smith, Christopher M. Rozoff, Timothy J. Wagner, David D. Turner[1], Wayne F. Feltz, Steven A. Ackerman

Cooperative Institute for Meteorological Satellite Studies, Space Science and Engineering Center, University of Wisconsin-Madison
[1]National Severe Storms Laboratory, National Oceanic and Atmospheric Administration

1. INTRODUCTION

Bores are a type of gravity wave that form when a density current interacts with a stable layer. In the atmosphere, bores frequently form as a result of thunderstorm outflow, or a cold front interacting with a nocturnal boundary layer (Crook 1988, Rottman and Simpson 1989). Studies have suggested that bores may destabilize the boundary layer, through alterations to the thermodynamic properties due to mixing, and permanent parcel displacements caused by the bore (eg. Koch et al. 2008, Coleman and Knupp 2011). Multiple cases have also been documented in which the lifting caused by a bore passage may have assisted in the convective initiation process (eg. Koch and Clark 1999, Coleman and Knupp 2011, Karyampudi et al. 1995).

The Plains Elevated Convection at Night (PECAN) field campaign, which took place from 1 June 2015 to 15 July 2015, aimed to gain a greater understanding and increase the forecast accuracy of nocturnal elevated convection. PECAN was a collaborative effort between multiple universities and private and government agencies and featured observations from a variety of fixed sites located in Nebraska, Kansas, and northern Oklahoma; aircraft observations; and mobile observations from Doppler radars, mesonets, remote sensing profiling units, and radiosonde launching systems. The science objectives of PECAN included: 1) advancing the knowledge of processes and conditions leading to initiation and early evolution of elevated convection, 2) understanding mesoscale convective system (MCS) internal structure and microphysics, 3) understanding the initiation, propagation and demise of bores and other mesoscale boundary layer wave-like features, and 4) improving the skill of storm- and MCS-scale numerical weather prediction. One of the underlying themes to these science objectives is identifying the instrumentation that is essential for observing and improving forecasts of these phenomena. More information on PECAN including further discussion of science objectives and operations planning can be found at: http://www.pecan15.org/home/PECANOperationsPlan.pdf.

This paper will present some initial work with various PECAN observations from two of the aforementioned mobile remote sensing profiling units. We will focus on displaying observations made by two of the mobile profiling units of an eastern Kansas bore on 26 June 2015.

2. DATA & INSTRUMENTATION

The Collaborative Lower Atmosphere Mobile Profiling System (CLAMPS), from the University of Oklahoma and National Severe Storms Laboratory, and the Space Science and Engineering Center (SSEC) Portable Atmosphere Research Center (SPARC), from the University of Wisconsin-Madison, were two of the mobile profiling units used during PECAN. These two mobile vehicles feature similar instrumentation suites, including an atmospheric emitted radiance interferometer (AERI) (Knuteson et al. 2004a,b), a 1.5 μm pulsed Doppler lidar (HALO Photonics, Great Britain; Pearson et al. 2009), radiosonde launching capabilities, and surface meteorology observations. The SPARC also features a High-Spectral Resolution Lidar (Razenkov 2010) as part of its instrument suite.

AERI measures downwelling infrared radiation between 3.3 and 19.2 μm at a spectral resolution of about 1 cm^{-1}. AERI observed radiances can be used to produce nearly continuous profiles of temperature and moisture in the bottom 2 km of the atmosphere using AERIoe (Turner and Löhnert 2014), an optimal estimation retrieval technique. First guesses for the retrieval were obtained from a radiosonde climatology from the Atmospheric Radiation Measurement Program's Southern Great Plains site in Lamont, Oklahoma. AERIoe also requires an input of cloud base height from an external instrument. For this campaign, cloud base height was determined by the backscatter profiles from the Doppler lidar. AERI-derived atmospheric soundings have been used in a variety of boundary layer studies (eg. Koch et al. 2008,

* *Corresponding author address:* David M. Loveless, Univ. of Wisconsin-Madison, Dept. of Atmospheric and Oceanic Sciences, Madison, WI 53726; e-mail: dloveless@wisc.edu.

Tanamachi et al. 2008, Demoz et al. 2006, Wagner et al. 2008).

The pulsed Doppler lidar uses a 1.5 μm pulse to remotely analyze boundary layer wind speed and direction. Naturally-occurring aerosols and clouds backscatter the transmitted 1.5 μm pulse. By considering the Doppler shift of the backscatter light, the along-beam component of the scatters' velocity can be determined. The vertical depth over which the lidar can measure winds is dependent on the aerosols in the atmosphere, which in turn is dependent on atmospheric state, geographic location, and the synoptic meteorology conditions. Velocity-aximuth display (VAD) wind profiles were obtained every two minutes by taking a complete aximuth scan at zenith angle of 30^{o}. In between VAD scans, the lidar pointed vertically to measure vertical winds.

Between the Doppler lidar and AERI, both kinematic (vertical and horizontal winds) and thermodynamic (temperature and moisture) profiles of the boundary layer were derived. The combination of these two instruments allows for a high-temporal resolution study of boundary layer phenomena during the PECAN campaign. Observations from each instrument and comparisons between the two mobile units will be made in the next section.

3. RESULTS AND OBSERVATIONS

25 – 26 June 2015 saw scattered convection throughout central Kansas along with a cluster of unorganized convection moving from west to east in northern Kansas ahead of a shortwave trough. CLAMPS and SPARC, along with the rest of the PECAN mobile fleet, were deployed in eastern Kansas to observe any bores that could form as a result of this convection (PECAN intensive observation period 16). Figure 1 displays the National Weather Service WSR-88D 0.5^{o} base reflectivity from Wichita, Kansas, at 0532 UTC, along with the location of CLAMPS and SPARC for that night. CLAMPS was located at 38.12^{o}N, 96.14^{o}W in Madison, Kansas, while SPARC was located at 37.83^{o}N, 96.28^{o}W in Eureka, Kansas. Convection in northern Kansas initiated a bore that propagated south-southeast over the mobile instruments. The small area of convection seen due west of CLAMPS, north of El Dorado, Kansas, was likely initiated by this bore, which was later observed by the CLAMPS and SPARC instrumentation.

3.1 *CLAMPS Observations*

As previously mentioned in section 2, the Doppler lidar and AERI can be used to produce high-temporal resolution observations of the boundary layer. Beginning with the CLAMPS observations of the bore, Figure 2 displays the AERIoe-derived potential temperature from 0300 UTC to 0920 UTC. The lifting of the bore is evident beginning around 0645 UTC, where the 305 K isentropic layer gets lifted from about 250 m to 700 m. Note, we will define the onset of the bore as 0645 UTC, as defined by the start of the isentropic layer lifting observed by the AERIoe retrievals. By 0745 UTC however, that layer has returned back to its original position and the temperature profile looks nearly identical to how it looked prior to the bore passage.

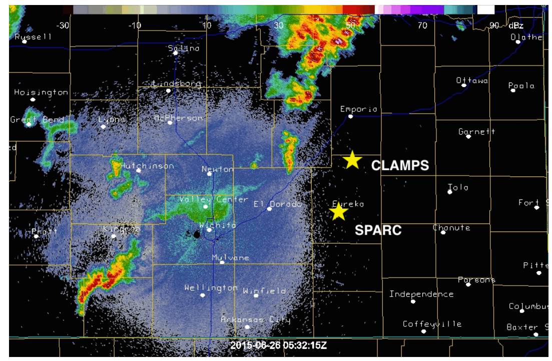

Figure 1. 0532 UTC 0.5^{o} base reflectivity from the Wichita Weather Service Doppler Radar on 26 June 2015. Locations of CLAMPS and SPARC are displayed with yellow stars.

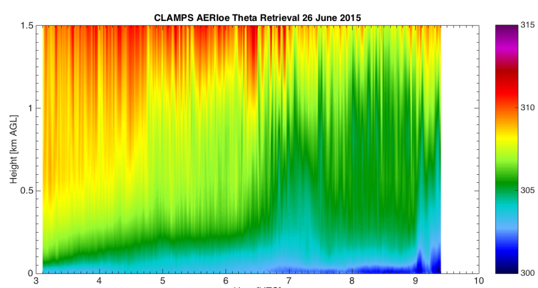

Figure 2. CLAMPS AERIoe derived potential temperature (K) from 0300 UTC to 0920 UTC.

Evidence of the bore can also be seen in the wind fields obtained by the Doppler lidar, as shown in Figure 3. A slight wind shift between 0630 and 0700 UTC can be seen in the lowest 500 m of the atmosphere. Additionally the winds below 500 m weaken with the bore passage. Only very weak upward velocities, around 0.1 m s^{-1}, are observed by the Doppler lidar at the onset of the bore at 0645 UTC. However by 0720 UTC, stronger upward velocities, peaking around 0.5 m s^{-1}, are observed, followed by upward/downward oscillations, with -0.5 m s^{-1} vertical velocities observed shortly thereafter. These upward and downward oscillations continue until 0845 UTC when a second bore arrives. While we will not focus on the second bore that CLAMPS observed, it is worth noting the difference in appearance in the Doppler lidar retrievals between the two bores observed by CLAMPS.

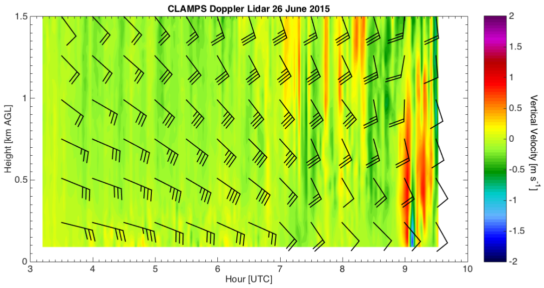

Figure 3. CLAMPS Doppler lidar retrievals from 0300 UTC to 0920 UTC. Wind barbs represent horizontal wind speed and direction, placed every 30 minutes temporally and every 0.25 km vertically. Shading represents vertical velocity (m s^{-1}).

The passage of the bore also changes the horizontal wind field. Figure 4 displays the horizontal wind speed retrievals from the Doppler lidar; the low-level jet (LLJ) is clearly visible over CLAMPS with the core of the jet clearly visible as wind speeds between 20 and 25 m s^{-1} centered around 500 m above ground level in advance of the bore. The onset of the bore is seen at 0645 UTC as the LLJ is lifted from 500 m to 1000 m above ground level, consistent with the timing of AERI observations of the bore onset, despite the seeming inconsistencies with the vertical velocity fields seen in Figure 3. Post-bore, the oscillations in the vertical wind filed are coincident with veriations seen in the horizontal wind field, as higher wind speeds from the LLJ core are able to be seen getting mixed towards the surface, particularly at 0730 UTC.

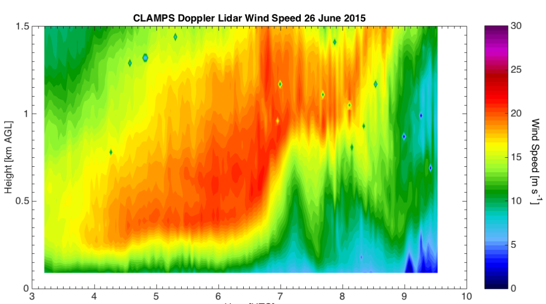

Figure 4. CLAMPS Doppler lidar retrieved horizontal wind speed (m s^{-1}) from 0300 UTC to 0920 UTC.

3.2 *SPARC Observations*

SPARC was located approximately 40 km south of CLAMPS, and was able to observe the same bore with the same suite of instrumentation. Beginning with SPARC's Doppler lidar retrievals in Figure 5, the onset of the bore is observed at 0730 UTC. Once again there is a wind shift and weakening of the winds in the horizontal in the lowest 500 m of the atmosphere. Additionally, a large spike in vertical velocities is observed in the vertical wind profile, with the onset of the bore, peaking around 1.5 m s^{-1}. This appearance in the bore passage on SPARC's Doppler lidar is quite different from the bore passage observed with the same instrument on CLAMPS, seen in Figure 3. CLAMPS' observations lacked that initial spike in vertical motion, observed by SPARC, however, CLAMPS observed vertical oscillations following the bore passage, while SPARC does not observe such a phenomena.

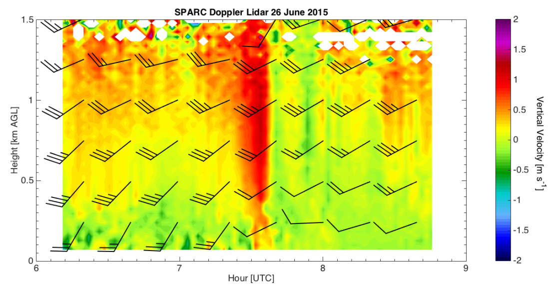

Figure 5. SPARC Doppler lidar retrievals from 0615 UTC to 0845 UTC. Wind barbs represent horizontal wind speed and direction, placed every 20 minutes temporally and every 0.25 km vertically. Shading represents vertical velocity (m s^{-1}).

Comparisons of the effect of the bore passage on the thermodynamic properties of the atmosphere can also be made when considering the AERIoe retrievals. Figure 3 displayed the AERIoe-derived potential temperature from CLAMPS, while Figure 6 displays the same for SPARC. CLAMPS observed a temporary lifting and later subsidence of the 305 K isentropic layer, while SPARC observes a quasi-permanent lifting (permanent at least to 75 minutes following the bore onset, which is the extent of SPARC's observations for the night) of the 305 K isentropic layer. Similar observations can be made between the two observing sites when considering the Doppler lidar retrieved horizontal wind field. Figure 4 shows CLAMPS observed horizontal wind speed, while Figure 7 displays SPARC observed horizontal wind speed. CLAMPS horizontal wind speeds would coincide with what is retrieved in the AERIoe potential temperature profiles (Figure 2), in that the 305 K layer subsides and higher wind speeds are seen to mix down from the lifted LLJ core. Between Figures 5 and 6, the 305 K layer and LLJ are lifted and stay lifted for the duration of the observing period for SPARC. Note also that the vertical velocity profiles from each observing site supports these observations, with CLAMPS observing some vertical oscillations following the bore, while SPARC did not observe any oscillations following the bore passage. This difference between the two profiling units, could possibly be explained using the AERIoe temperature retrievals from CLAMPS and SPARC, seen in Figures 8 and 9 respectively. From Figures 8 and 9, it is evident that the low-level inversion is stronger over CLAMPS than over SPARC. The higher stability in the boundary layer over CLAMPS would promote the vertical oscillations that were observed in the Doppler lidar retrievals with CLAMPS. However, additional analysis is required to understand these differences in a more complete and quantitative manner.

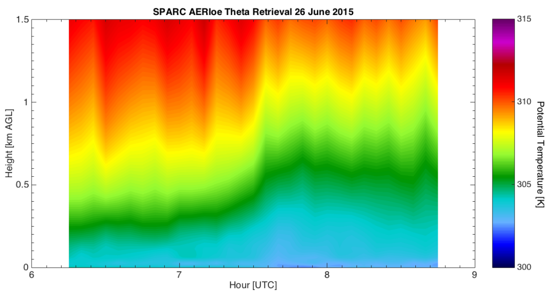

Figure 6. SPARC AERIoe derived potential temperature (K) from 0615 UTC to 0845 UTC.

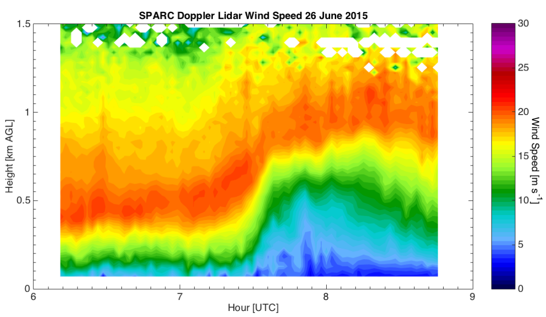

Figure 7. SPARC Doppler lidar retrieved horizontal wind speed (m s^{-1}) from 0615 UTC to 0845 UTC.

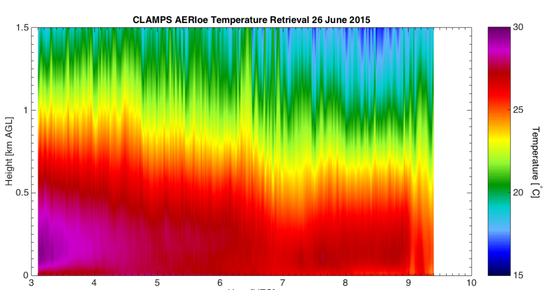

Figure 8. CLAMPS AERIoe derived temperature (°C) from 0300 UTC to 0920 UTC.

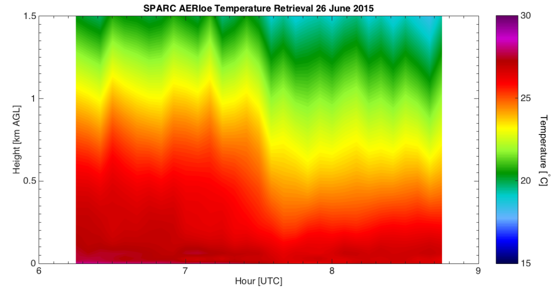

Figure 9. SPARC AERIoe derived temperature (°C) from 0615 UTC to 0845 UTC.

Between the AERI and Doppler lidar, comparisons of the same bore, passing each observing site approximately 45 minutes apart, interesting comparisons are able to be made. Using a time of 45 minutes and estimating the bore orientation to be exactly WSW (line between 67.5° and 247.5° from north) a bore speed of 8.56 m s^{-1} can be calculated. This observed speed can be compared to hydraulic theory using the following equation for bore speed derived by Rottman and Simpson (1989):

$$C_{bore} = C_{gw}\left[\frac{1}{2}\frac{h_1}{h_0}\left(1+\frac{h_1}{h_0}\right)\right]^{\frac{1}{2}} \qquad (1)$$

where h_0 is the depth of the surface fluid prior to the bore passage, h_1 is the depth of the surface fluid following the bore passage, and C_{gw} can be derived to be:

$$C_{gw} = \left[g\left(\frac{\Delta\theta_v}{\theta_v}\right)h_0\right]^{\frac{1}{2}} \qquad (2)$$

where θ_v is the average potential temperature across the inversion, and $\Delta\theta_v$ is the difference in average potential temperature above and below the inversion. Using the SPARC radiosondes launched prior to and following the bore to calculate h_0 and h_1, and the pre-bore radiosonde to calculate θ_v and $\Delta\theta_v$, C_{bore} is calculated to be 10.36 m s^{-1}. Considering the approximation for bore orientation made deriving the observed bore speed, these two values are quite close to each other, meaning hydraulic theory would appear compare well to observations for this case.

The identical instrumentation on each observing vehicle reduces differences how the bore is observed, meaning that observed changes in the bore are likely due to its evolution and the local environment. Clearly, high-temporal resolution temperature and wind profilers are important tools for observing bore structure and evolution. These observations would benefit operational forecasters in understanding the effect the bore passage is having on the local boundary layer, which is important for diagnosing potential convective initiation.

3.3 *SPARC Radiosonde Observations*

By design during the intensive observation period, SPARC launched two radiosondes near the bore passage. From Figures 5, 6, and 7, it is evident the bore passage occurred around 0730 UTC. SPARC launched one radiosonde at 0707 UTC, representative of the pre-bore environment, and another radiosonde at 0752 UTC, representative of the post-bore environment. The temperature and dew point temperature profiles of these two radiosondes are displayed in Figure 10.

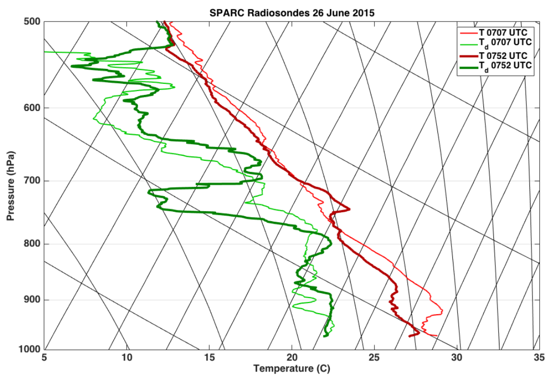

Figure 10. Skew-T log-P diagram of two SPARC radiosondes launched at 0707 UTC (pre-bore, thin lines) and 0752 UTC (post-bore, bold lines). Temperature for each radiosonde is represented by the red lines, dew point temperature for each radiosonde is represented by the green lines.

Two important observations about the bore passage can be made when considering the differences between the pre- and post-bore soundings. A low level inversion, and thus a stable boundary layer (a necessary condition for bores) is evident on the pre-bore sounding. However, that inversion is lifted dry adiabatically from 925 hPa to 875 hPa with the bore passage, validating the lifting that was previously identified using ground-based remote sensing instruments. Additionally, that lifting of the capping inversion reduces the low-level convective inhibition, which could help promote convective initiation later on. The two radiosonde launches also provide evidence of the mixing that occurred in the boundary layer with the bore passage. This is evident when considering the dew point temperature profile of the two soundings in Figure 10. While the pre-bore environment has varying moisture levels in the boundary layer, the post-bore sounding shows that the dew point temperature line is following a line of near-constant water vapor mixing ratio, indicating that the moisture in the boundary layer has become well mixed.

4. CONCLUSIONS

To summarize, the lifting observed by radiosondes in the pre- and post-bore environment was also observed by ground-based remote sensing instruments, AERI and Doppler lidar, on CLAMPS and SPARC. Note in Figure 1, that the bore observed by both CLAMPS and SPARC is outside of the clear air return region of the Wichita radar. As a result, this bore is unable to be identified on radar. However, the observations shown here would help identify bores outside of the clear air return region of a radar should a national network of atmospheric profilers be deployed in the future.

Future work on this project includes understanding the bore's potential role in convective initiation in the area. Additionally, further analysis is necessary to more completely understand the causes of the differences in the bore passages at each observing location.

Acknowledgment

This work was supported under NSF Atmospheric and Geophysical Science grant award number 1356914.

References

Coleman, T. A., and K. R. Knupp, 2011: Radiometer and profiler analysis of the effects of a bore and a solitary wave on the stability of the nocturnal boundary layer. *Mon. Wea. Rev.*, 139, 211-223.

Crook, N. A., 1988: Trapping of low-level internal gravity waves. *J. Atmos. Sci.*, 45, 1533-1541.

Demoz, B., and Coauthors, 2006: The dryline on 22 May 2002 during IHOP_2002 convective-scale measurements at the profiling site. *Mon. Wea. Rev.*, 134, 294-310.

Karyampudi, V. M., S. E. Koch, C. Chen, J. W. Rottman, and M. L. Kaplan, 1995: The influence of the Rocky Mountains on the 13-14 April 1986 severe weather outbreak. Part II: Evolution of a prefrontal bore and its role in triggering a squall line. *Mon. Wea. Rev.*, 123, 1423-1446.

Knuteson, R. O. and Coauthors, 2004: Atmospheric emitted radiance interferometer. Part I: Instrument design. *J. Atmos. Oceanic Technol.*, 21, 1763-1776.

Knuteson, R. O. and Coauthors, 2004: Atmospheric emitted radiance interferometer.

Part II: Instrument performance. *J. Atmos. Oceanic Technol.*, 21, 1777-1789.

Koch, S. E., and W. L. Clark, 1999: A nonclassical cold front observed during COPS-91: Frontal structure and the process of severe storm initiation. *J. Atmos. Sci.*, 56, 2862-2890.

Koch, S. E, W. F. Feltz, F. Fabry, M. Pagowski, B. Geerts, K. M. Bedka, D. O. Miller, and J. W. Wilson, 2008: Turbulent mixing processes in atmospheric bores and solitary waves deduced from profiling systems and numerical simulation. *Mon. Wea. Rev.*, 136, 1373-1400.

Pearson, G., F. Davies, and C. Collier, 2009: An analysis of the performance of the UFAM pulsed Doppler lidar for observing the boundary layer. *J. Atmos. Oceanic Technol.*, 26, 240-250.

Razenkov, I., 2010: Characterization of a Geiger-mode avalanche photodiode detector for high spectral resolution lidar. M.S. Thesis, Dept. of Atmospheric and Oceanic Sciences, University of Wisconsin-Madison, 72 pp.

Rottman, J. W., and J. E. Simpson, 1989: The formation of internal bores in the atmosphere: a laboratory model. *Q. J. R. Meteorol. Soc.*, 115, 941-963.

Tanamachi, R. L., W. F. Feltz, and M. Xue, 2008: Observations and numberical simulation of upper boundary layer rapid drying and moistening events during the International H_2O Project (IHOP_2002). *Mon. Wea. Rev.*, 3106-3120.

Turner, D. D., and U. Löhnert, 2014: Information content and uncertainties in thermodynamic profiles and liquid cloud properties retrieved from the ground-based atmospheric emitted radiance interferometer (AERI). *J. Appl. Meteor. Climatol.*, 53, 752-771.

Wagner, T. J., W. F. Feltz, and S. A. Ackerman, 2008: The temporal evolution of convective indices in storm-producing environments. *Wea. Forecasting*, **23**, 786-794.